LEGIBILITY NOTICE

A major purpose of the Technical Information Center is to provide the broadest dissemination possible of information contained in DOE's Research and Development Reports to business, industry, the academic community, and federal, state and local governments.

Although a small portion of this report is not reproducible, it is being made available to expedite the availability of information on the research discussed herein.

LA-UR -88-963

CONF-880693--1

Los Alamos National Laboratory is operated by the University of California for the United States Department of Energy under contract W-7405-ENG-36

LA-UR--88-963

DE88 007827

TITLE FREELY EXPANDING DETONATION PRODUCTS: SCALING OF RATE PROCESSES

AUTHOR(S) N. Roy Greiner

SUBMITTED TO 19th International ICT Conference on Combustion and Detonation

June 29--July 1, 1988
Karlsruhe, Federal Republic of Germany

Los Alamos National Laboratory
Los Alamos, New Mexico 87545

FREELY EXPANDING DETONATION PRODUCTS: SCALING OF RATE PROCESSES

N. Roy Greiner

Chemical and Laser Sciences Division
Los Alamos National Laboratory
Los Alamos, New Mexico, USA 87545

Abstract

Using the Los Alamos reactive hydrodynamics code KIVA, calculations have been made to simulate the free expansion of cylinders of detonation products into a high vacuum. The emphasis of this paper is on the scaling of rate processes with cylinder size and initial conditions as a function of position in the expanding mass. The processes considered include diffusion, unimolecular decomposition, bimolecular radical reactions, and vibrational relaxation. The calculations also give time-dependent velocity fields; schlieren images; and profiles of density, pressure, and temperature. Many features of the calculations can be compared with experimental observations, including time-delayed schlieren and shadowgraph snapshots, time-dependent absorption spectra, and time-of-arrival profiles of molecular species. Some unexpected insights, such as the effect of the equation of state on the shape of the expanding plume and the effect of position on the rate of quenching, will be discussed.

These calculations are being used to interpret the available experimental data and to design future experiments.

1. INTRODUCTION

This effort was undertaken to provide insight into a number of experiments involving the characterization of the chemical products of detonations carried out in chambers maintained at vacuum[1,2] or at very low pressures compared with detonation pressures.[3] Free expansion of detonation products provides a means for the chemical characterization of detonation because reactions occurring in the detonating material are quenched by the reduction in both collision frequency and collision intensity as the result of adiabatic expansion. As the product plume expands, the mean free path of the molecules becomes longer, until it is possible to skim a collisionless molecular beam of the quenched reacting molecules for analysis. If negligible scrambling of the molecules occurs during the detonation and expansion, then the molecular beam provides a continuous chemical history of the detonation and quenching processes. Therefore, for our purposes, an essential feature of the free-expansion process is that diffusive mixing occurs only to a negligible degree before the beam is analyzed. This feature allows one to map arrival time of the molecular beam at a detector, such as a mass spectrometer, back to the position in the original charge. With an experimentally verified model of the hydrodynamics of the expanding plume, a hydrodynamic history can be linked with the chemical composition of the beam arriving at the detector during any time segment. Such information can be used to construct and test models of the chemical mechanism of detonation processes. This paper describes initial efforts to provide such a model.

2. DESCRIPTION OF THE MODEL

The KIVA code is a reactive hydrodynamics code for treating fluids with embedded chemical reactions taking place with gas-phase and condensed-phase reactants and products.[4] The code uses a Lagrangian mesh and computational methods that are well suited for modeling the free expansion of reacting hot, dense fluids into a high vacuum.

For these initial studies, we have chosen a simple problem that ignores some minor characteristics of a detonating charge. For simplicity, we assume a cylinder of hot, dense fluid with no density gradients and no initial velocity components that sits on an immovable slab of infinite extent in the radial direction. The fluid is assumed to have an equation of state (EOS) corresponding to the adiabatically expanding detonation products of PETN. The EOS used here is fashioned to fit the calculated Becker-Kistiakowski-Wilson EOS at high density and the ideal gas adiabat at low density. When a simple single-term gamma-law EOS was used, the low-density regime was not accurately modeled, making the plume cone-shaped, but with the two-term EOS, the shape is more rounded as is observed experimentally. The initial values and the EOS for all computations referred to in this paper are summarized in Table I.

TABLE I

INITIAL CONDITIONS AND THE EQUATION OF STATE

Charge Shape:	Right circular cylinders having equal diameters and heights, noted in the text by the dimension of their diameters
Initial Density:	$d\ (g/cm^3) = 1.67$
Initial Pressure:*	$P\ (dyne/cm^2) = 1.24 \times 10^{11}$
Pressure:	$P = 2.53 \times 10^{10}\ d^{2.8} + 8.73 \times 10^{9}\ d^{1.4}$
Temperature:	$T(K) = 2287\ d^{0.4}$

*10^{11} dyne/cm^2 = 100 kbar = 10 GPa

A computational mesh with 20 cells across the diameter and 20 cells along the cylinder axis (Z-axis) is embedded in the cylinder. During the computation, no mass flows between the cells; therefore, the mesh expands with the fluid during the computation. The mesh, at a very early time in the expansion (0.03 microsec), is shown in Fig. 1. During the following discussion, cells at several positions will be referred to in order to illustrate their expansion histories. Comparisons will be made between different positions in the same charge and comparable positions in different sizes of charges. The indices of these positions are pointed out in Fig. 1. Mesh and velocity fields and the density, pressure, and temperature profiles are shown as planar slices through the cylinder, which contain the axis and a diameter of the cylinder. The schlieren and shadowgraph images are projections of functions evaluated along lines passing through the cylinder. The lines, perpendicular to the plane mentioned above, pass through the cylinder and the centers of the cells as they are intersected by the plane.

3. RESULTS AND DISCUSSION

Figure 2 shows the mesh and velocity field of the 3-mm cylinder 0.9 microsec after expansion begins. Expansion has already begun throughout the cylinder, and the mesh is distorted considerably from its original shape (compare with Fig. 1). The maximum velocity in the Z-direction is already 5.78 mm/microsec, compared with the terminal velocity of 6.02 mm/microsec. Figure 3 shows the density and temperature profiles at 0.9 microsec. The contours are of logarithmic values (always to the base 10) of the density and temperature to show clearly the broad range of values. It is obvious that the temperature and density maps are superimposable. This is a direct result of the temperature being a simple exponential function of the density (see Table I) and the contours being logarithmic. This feature of these plots can

often be used to advantage in scaling and interpolating results, particularly after the flow becomes self-similar.

Figure 4 shows the mesh and velocity field for the 3-mm charge at 4.26 microsec. Comparison of this velocity field and later ones shows that the flow is now nearly self-similar, that is, the autoscaled mesh, velocity fields, and contour plots are nearly superimposable with all later ones (of the same type). The actual values of the density, pressure, and temperature decrease steadily as the fluid expands, but the shape of both the autoscaled mesh and the velocity field become invariant with time. The values on the temperature (Fig. 5) and pressure (Fig. 6) contour plots also steadily decrease during expansion, but their autoscaled contour plots become superimposable at all later times. At low values of the density, the pressure, as well as the temperature, becomes a simple exponential function of density. The first term in the pressure expression in Table I becomes vanishingly small compared with the second term at low densities, making the pressure a simple exponential function of the density.

Schlieren image contours, shown in Fig. 7, are computed for the 3-mm charge at 0.5 microsec and 2.5 microsec. These results show that schlieren images can be used to follow the size and shape of the plume as it expands into the vacuum and that an image taken through an aperture of 0.75×10^{-8} radian will show the edge of the expanding front quite faithfully during the first 2.5 microsec of expansion. Computed images for larger apertures (contours of higher value in Fig. 7) and later times suggest that other details of the density distribution can be observed as a function of time to provide hydrodynamic data for the expansion process. A system that uses a pulsed laser with variable delay after charge ignition has been tested on several charges, producing experimental schlieren images that can be compared with the computed ones.[5]

Fields of deflection vectors for a beam of light passing through the plume are generated by the code to compute the schlieren images. With some additional computation, these fields can be used for computing shadowgraph images at various distances from the plume to provide additional detail in the plume density profiles. Preliminary experimental results have also been obtained with shadowgraph images.[5] Work continues on the comparison of the experimental and computed images.

Other contour plots have been made, which include vibrational temperature of vibrationally excited product molecules,[6] time scales for elementary reactions using Arrhenius kinetics, mean free path of molecules, and mean distance for molecular diffusion during the expansion process. A typical computation gives a set of some 200 such mesh, contour, and vector plots. Value files of the above parameters are also produced for selected cells (see Fig. 1) as a function of time. We now examine illustrative plots of some of these parameters.

Figures 8-13 show values of several useful parameters for particular cells in cylinders ranging in size from 3 mm to 30 mm. From plots like these, it is possible to make comparisons of the parameter values at selected positions within a given charge and at similar positions in

charges of different sizes. It is also possible to derive from these plots simple relations that can be used to interpret experimental results, to scale experiments, and to design new experiments. Table II shows some expressions derived for cell (1,20) from the 3-mm charges typical of laboratory-scale studies of the chemistry of detonation products.[1,2,6]

TABLE II

SIMPLE EXPRESSIONS FOR PLUME CHARACTERISTICS AS A FUNCTION OF TIME AFTER 3 MICROSEC FOR CYL03, CELL (I = 1, K = 20)

Density:*	$d\ (g/cm^3) = d_0\ (t/0.4)^{-3}$
Pressure:	$P\ (dyne/cm^2) = P_0\ (t/0.25)^{-4.2}$
Temperature:	$T\ (K) = T_0\ (t/0.4)^{-1.2}$
Diffusion:	$DZ\ (cm) = 3 \times 10^{-6}\ (t/1.0)^{1.75}$
Mean Free Path:	$MFP\ (cm) = 1 \times 10^{-7}\ (t/1.0)^3$
Expansion Front:	$Z_{top}\ (cm) = 0.2 + 0.603\ t$

*Here t is in microsec; d_0, P_0, and T_0 are the initial values before expansion.

Density is useful for estimating the amount of material available for analysis in the molecular beam at the mass spectrometer and for the estimation of rates of collisional processes such as bimolecular reactions and vibrational-translational relaxation.[6] Pressure is important in determining the dynamics of the gas flow as the plume expands. Temperature is very important for chemical reactivity of species in the expanding plume. Values for mean free path are necessary for positioning the skimmer and the mass spectrometer ion source. Values of the mean distance of diffusion give estimates of one possible source of scrambling of the detonation products among cells. For example, the arrival time at the mass spectrometer of cell (1,20) from the 3-mm charge is 150 microsec, at which time the diffusion distance is 0.3 mm (Fig. 8). The product velocity of 6 mm/microsec gives an arrival-time scrambling of 0.05 microsec, a negligible value. This result implies that, with knowledge of the hydrodynamics, arrival time can be mapped back to precise positions in the expanding charge.

Characteristic e-folding times for a unimolecular and a bimolecular reaction are also displayed in Figures 8-13. Arrhenius functions are used with nominal parameters chosen for illustration. The functions shown in the figures are

$$\log \text{TUNI} = (E_a/4.6\ T_0)(d_0/d)^{0.4} - \log A, \text{ and}$$

$$\log \text{TBIM} = (E_a/4.6\ T_0)(d_0/d)^{0.4} - \log A - \log d - \log n,$$

where TUNI and TBIM are given in seconds. In the first equation, E_a is 40 000 cal/mol and A is 10^{16} sec^{-1}. In the second equation, E_a is 10 000 cal/mol, A is 10^9 l/mol-sec, d is in g/cm^3, T is in K, and n is 3 mol of critical reactant per kg. The zero subscripts refer to initial conditions. In the figures, a line segment is drawn through the plots of TUNI and TBIM to show approximately where reactions described by these functions would quench. For example, in the case of CYL03 (10,20) in Fig. 11, both reactions quench at 0.2 microsec, whereas at the other extreme for CYL30 (1,10) in Fig. 13, they quench at about 20 microsec. This illustrates the broad range of cooking times available for the investigation of reactions in detonations. As one proceeds inward from the face of CYL03 along the Z-axis, the quench time increases from 0.8 microsec at cell (1,20) (Fig. 8), to 1.0 microsec at cell (1,15) (Fig. 9), to 1.2 microsec at cell (1,10) (Fig. 10). As the size of the charge increases, the quench time for cell (1,10) in the charge interior increases from 1.2 microsec in CYL03 (Fig. 10), to 3.9 microsec in CYL10 (Fig. 12), to 13.9 microsec in CYL30 (Fig. 13). Thus, a broad range of reaction times are available for investigation as a function of charge size and position in the charge. These results also suggest that investigation of the most rapid processes might take advantage of the very rapid quenching at the cylinder corner cell (10,20) (Figs. 2, 4, and 11).

4. CONCLUSIONS

We conclude that this comoutational model gives useful results for interpreting and designing experiments on freely expanding detonation products. The present results provide a set of base-line computations useful for estimating the effects of scaling in these experiments. With future refinements, we expect to model finer details of these and more sophisticated experiments to derive information useful for designing explosive systems based on a more fundamental understanding of detonation chemistry.

5. ACKNOWLEDGEMENTS

Peter O'Rourke and Tony Amsden provided much assistance in adapting the KIVA code for this work. Sc. . Murray assisted in running the code and provided much of the output graphics. Discussions with Norm Blais about many aspects of free-expansion experiments were most beneficial.

6. REFERENCES

1. N. Roy Greiner and Normand Blais, "Real-time Analysis of the Chemical Products form Shocked Nitric Oxide," Proceedings of the 17th International Annual Conference of ICT, Fraunhofer-Institut fur Treib-und Explosivstoffe (ICT), Karlsruhe, Federal Republic of Germany, 1986, p. 33-1.

2. N. Blais, "Real-time Analysis of HNS Detonation Products: Carbon clusters," J. of Energetic Materials 5, 57 (1987).

3. J. D. Johnson, N. R. Greiner, D. Phillips, and F. Volk, "Diamond Clusters in Detonation Soot," Meeting of the American Physical Society, March 21-25, 1988, New Orleans, Louisiana, Paper M218.

4. A. A. Amsden, J. D. Ramshaw, P. J. O'Rourke, and J. K. Dukowicz, "KIVA: A Computer Program for Two- and Three-Dimensional Fluid Flows with Chemical Reactions and Fuel Sprays," Los Alamos National Laboratory report LA-10245-MS (February 1985).

5. Normand C. Blais, private communication.

6. Normand C. Blais and N. Roy Greiner, "Real-Time Analysis of the Reaction Products of Shocked Nitric Oxide," submitted to J. Energetic Materials.

Figure 1. Computational mesh for the 3-mm cylinder at 0.03 microsec. Top and edge cells have expanded just noticeably. Z_{top} = 3.05 mm. Figs. 1-6 are autoscaled to the corresponding value of Z_{top}. Location A corresponds to cell (1,20), B to (1,15), C to (1,10), and D to (10,20).

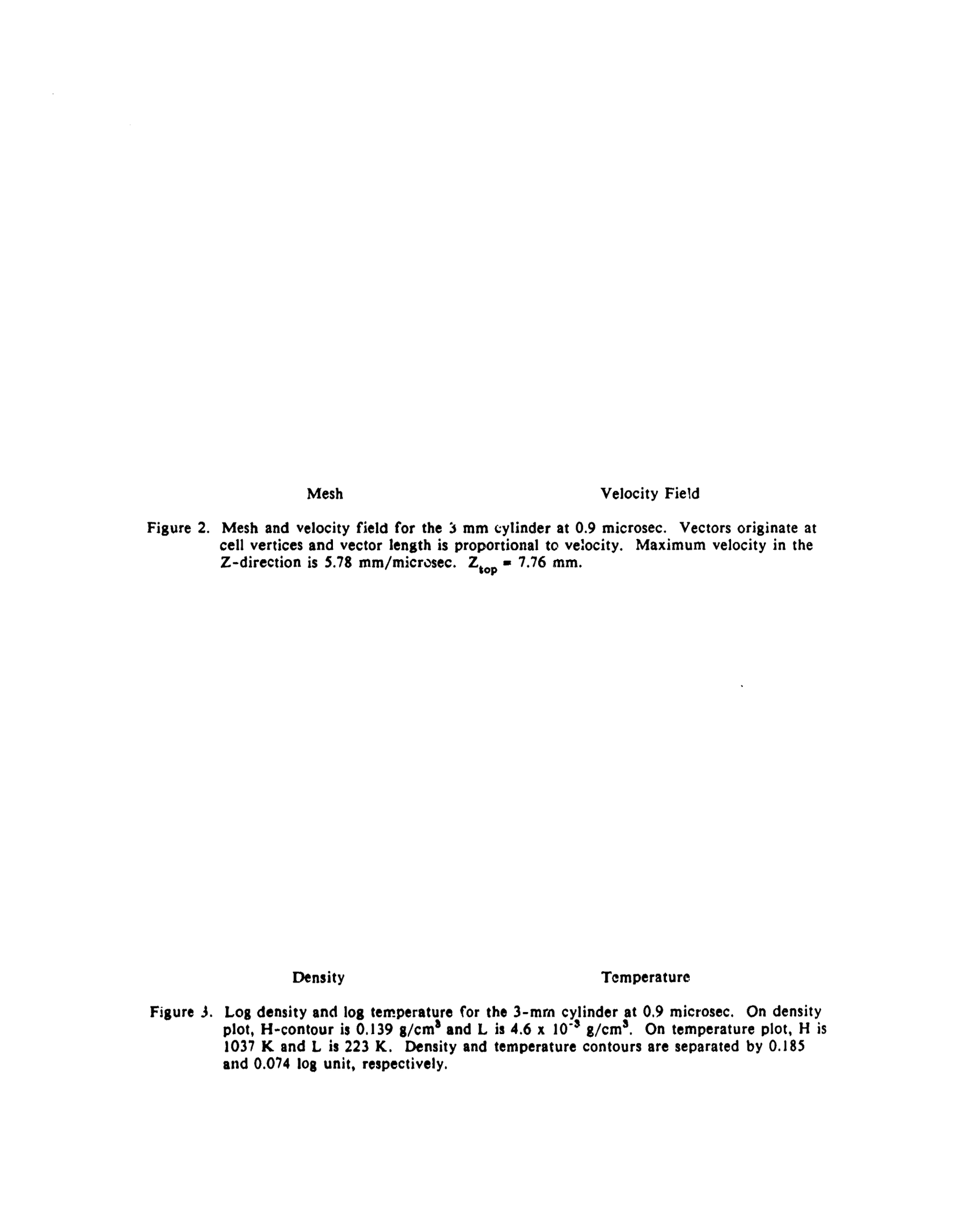

Figure 2. Mesh and velocity field for the 3 mm cylinder at 0.9 microsec. Vectors originate at cell vertices and vector length is proportional to velocity. Maximum velocity in the Z-direction is 5.78 mm/microsec. Z_{top} = 7.76 mm.

Figure 3. Log density and log temperature for the 3-mm cylinder at 0.9 microsec. On density plot, H-contour is 0.139 g/cm^3 and L is 4.6 x 10^{-3} g/cm^3. On temperature plot, H is 1037 K and L is 223 K. Density and temperature contours are separated by 0.185 and 0.074 log unit, respectively.

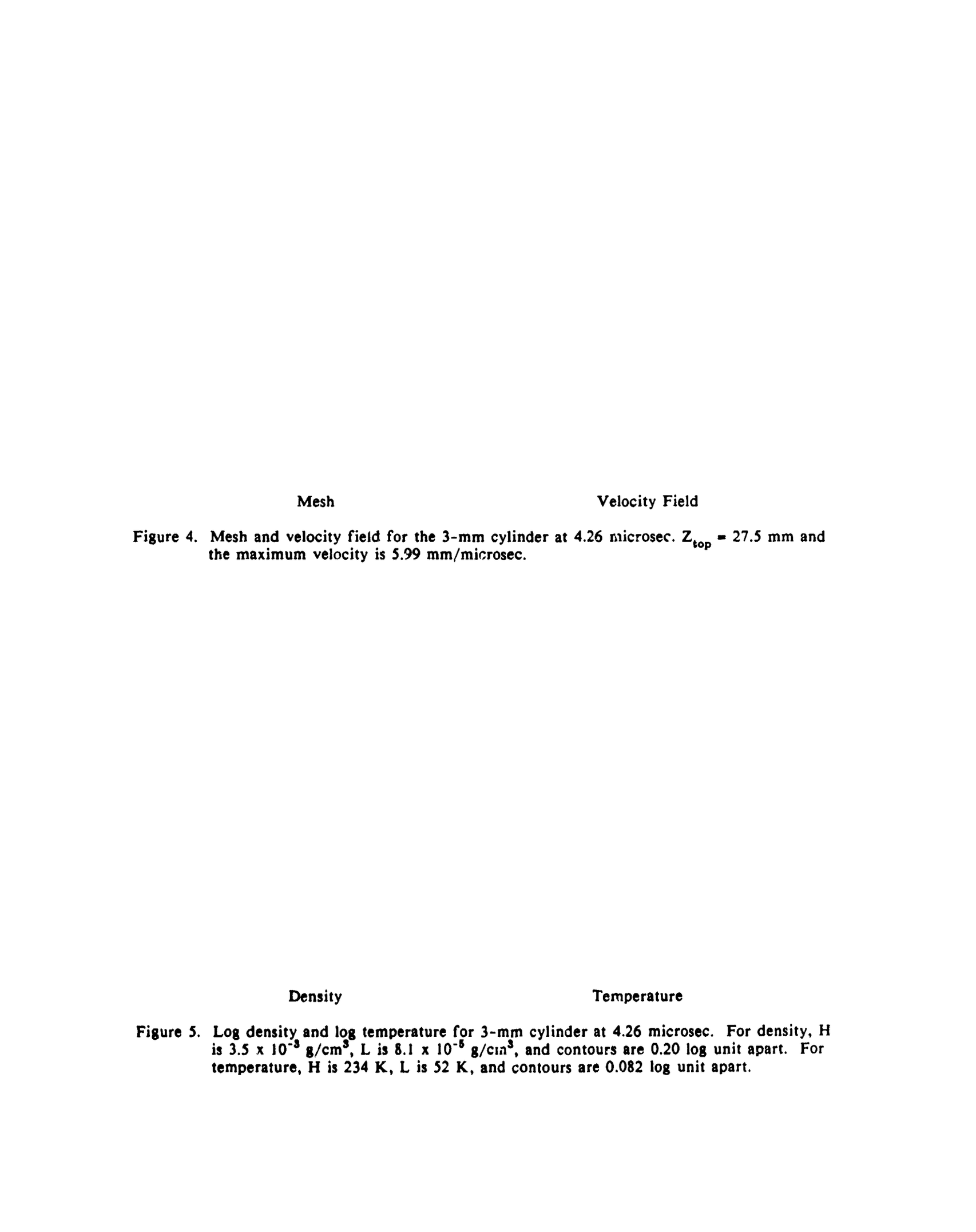

Figure 4. Mesh and velocity field for the 3-mm cylinder at 4.26 microsec. Z_{top} = 27.5 mm and the maximum velocity is 5.99 mm/microsec.

Figure 5. Log density and log temperature for 3-mm cylinder at 4.26 microsec. For density, H is 3.5 x 10^{-3} g/cm^3, L is 8.1 x 10^{-5} g/cm^3, and contours are 0.20 log unit apart. For temperature, H is 234 K, L is 52 K, and contours are 0.082 log unit apart.

0.9 microsec 4.26 microsec

Figure 6. Log pressure for 3-mm cylinder at 0.9 and 4.26 microsec. For 0.9 microsec, H is 7.1 x 10^8 dyne/cm^2, L is 4.8 x 10^6 dyne/cm^2, and contours are 0.27 log unit apart. For 4.26 microsec, H is 3.1 x 10^6 dyne/cm^2, L is 1.6 x 10^4 dyne/cm^2, and contours are 0.29 log unit apart.

0.5 microsec 2.6 microsec

Figure 7. Schlieren image contours computed for the 3-mm cylinder at 0.5 and 2.6 microsec. For the 0.5-microsec image, H is a deflection angle of 0.10 radian, L is 5.0 x 10^{-3} radian, and contours are 1.26 x 10^{-2} radian apart. For the 2.6-microsec image, H is 1.55 x 10^{-2} radian, L is 7.5 x 10^{-4} radian, and contours are 1.86 x 10^{-3} radian apart. Images have been obtained experimentally with a system having an aperture of 7.5 x 10^{-4} radian, so the L contour in the computed image would correspond closely to the edge of the experimental image at 2.6 microsec. At 0.5 microsec, Z_{top} = 5.6 mm and, at 2.5 microsec, 17.5 mm.

Figure 8. Values for various parameters of the expanding products from position A (Fig. 1), cell (1,20), in the 3-mm charge as a function of time. Units are cm-g-sec units. d = density. P = pressure, DZ = mean diffusion distance, T = temperature, MFP = mean free path, TBIM = reaction time for the bimolecular reaction, TUNI = reaction time for the unimolecular reaction.

Figure 9. Parameters for 3-mm cylinder, position B, cell (1,15).

Figure 10. Parameters for 3-mm cylinder, position C, cell (1,10).

Figure 11. Parameters for 3-mm cylinder, position D, cell (10,20).

Figure 12. Parameters for a 10-mm cylinder, position C, cell (1,10).

Figure 13. Parameters for the 30-mm cylinder, position C, cell (1,10).

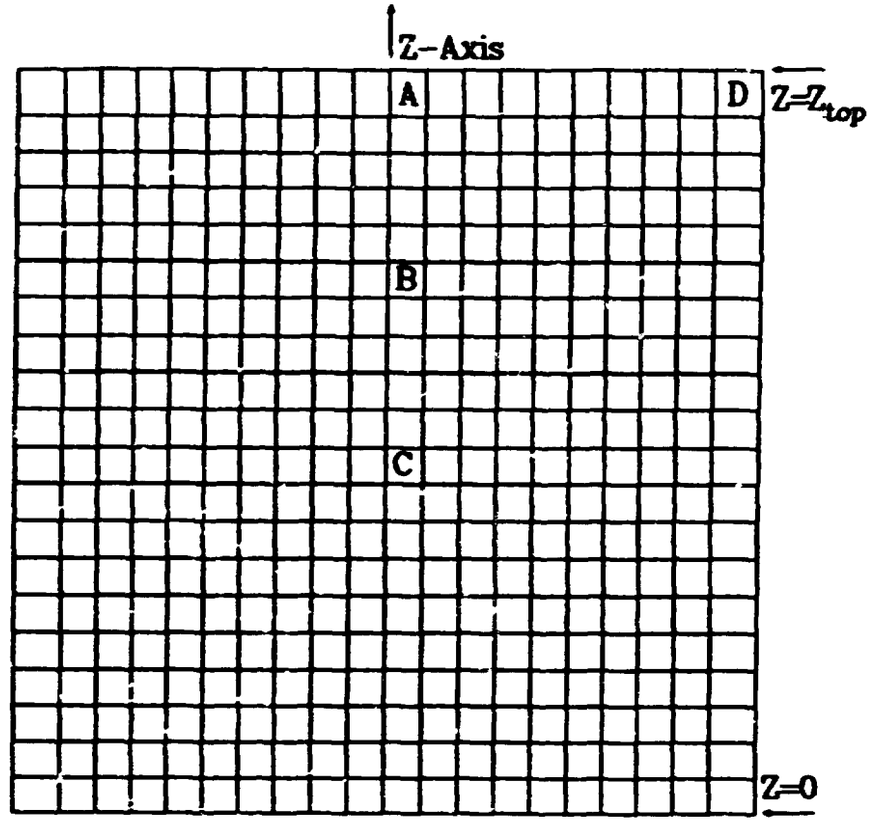

Fig.1.

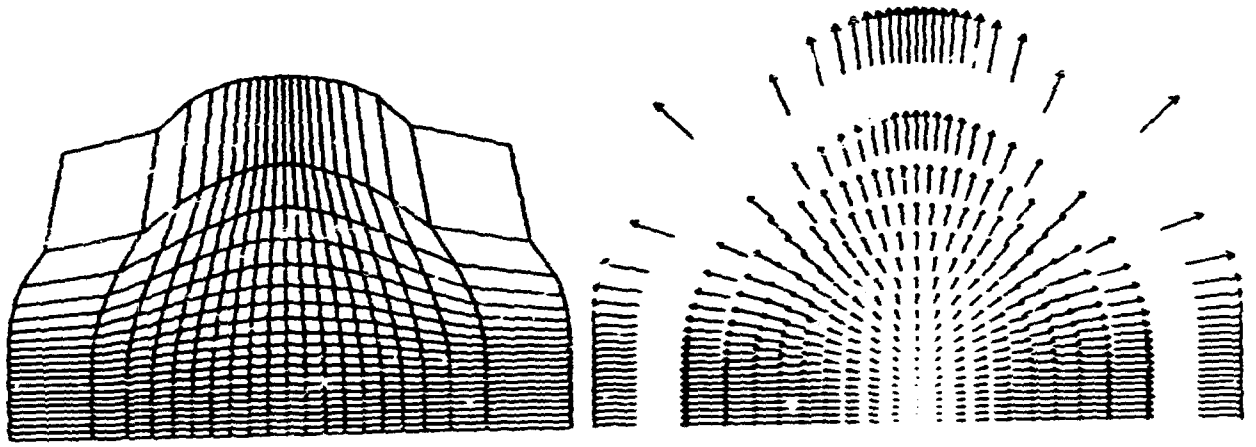

Fig. 2.

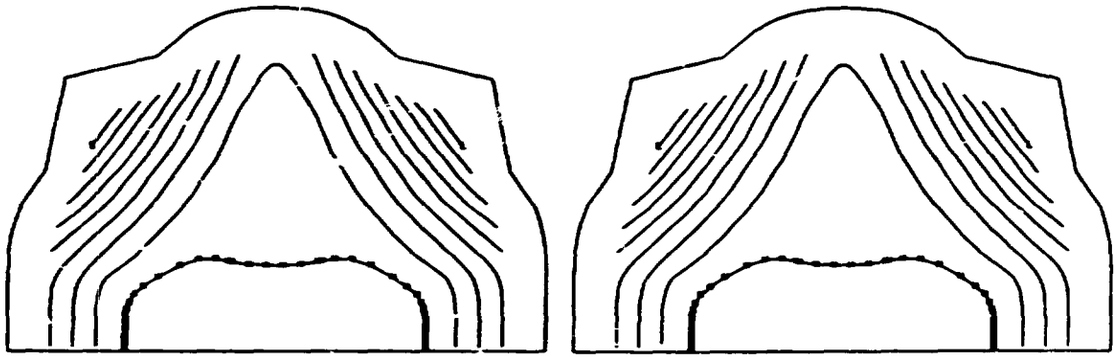

Fig. 3.

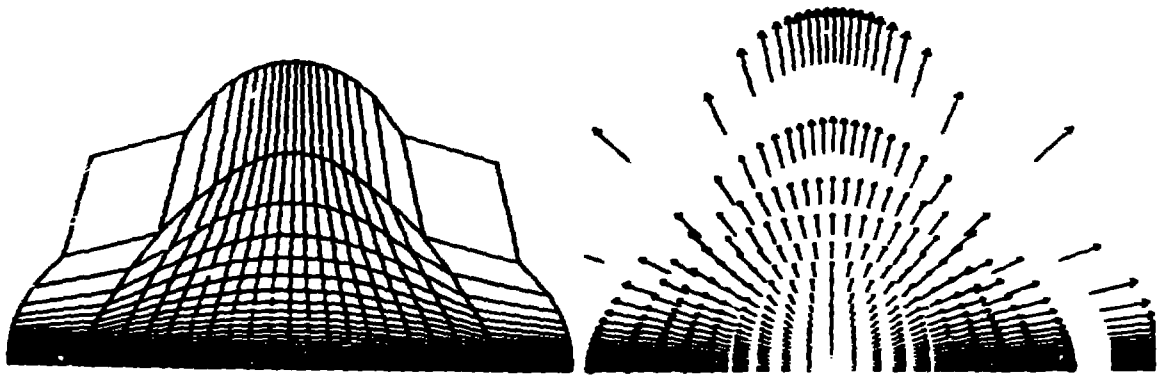

Fig.4.

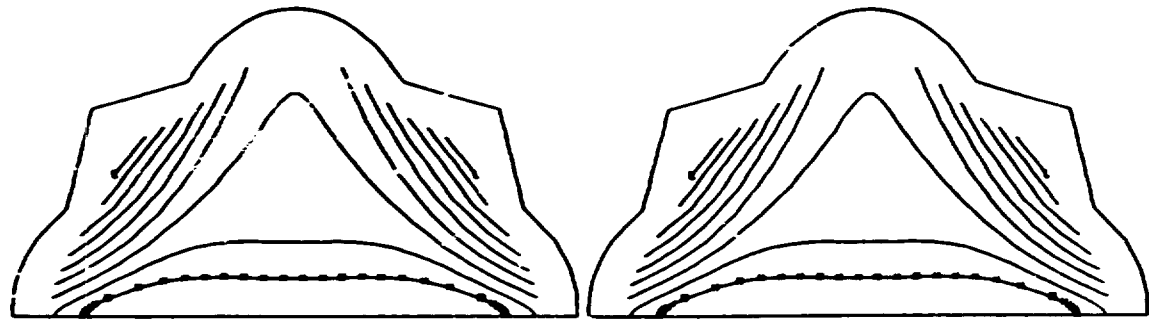

Fig. 5.

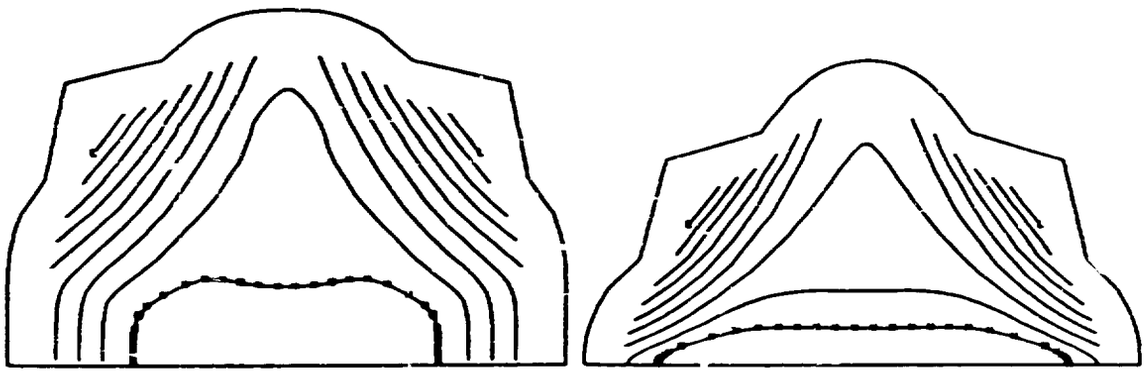

Fig. 6.

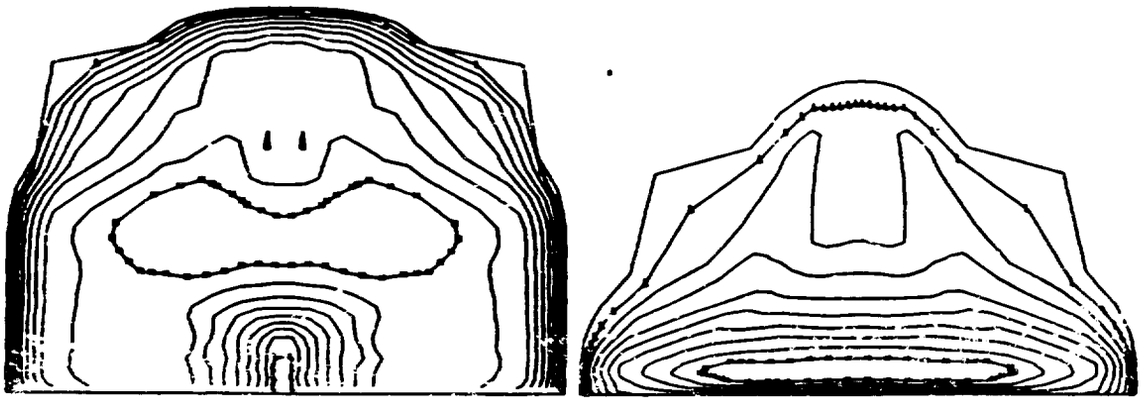

Fig. 7.

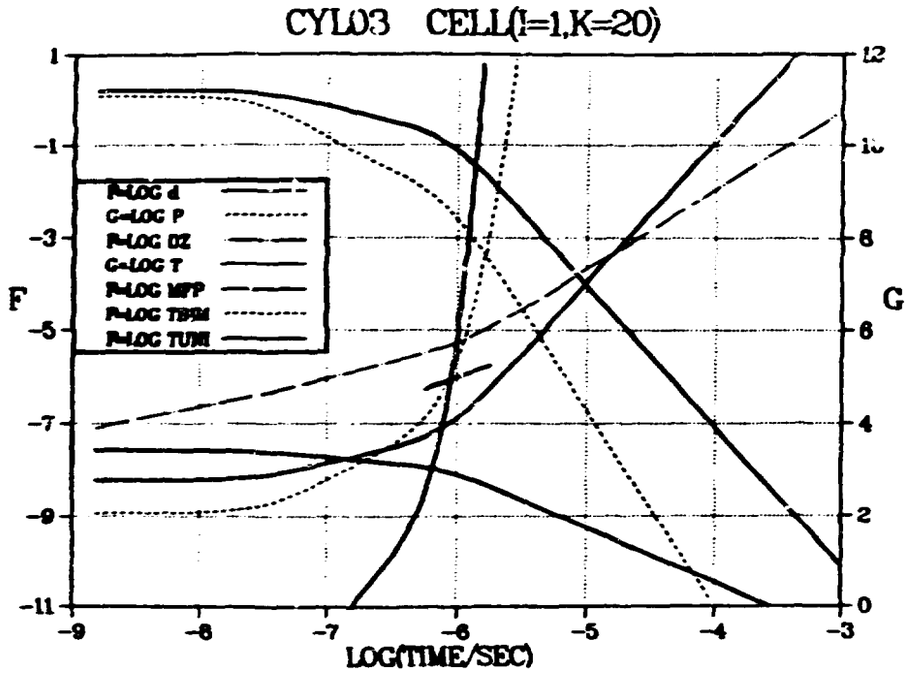
CYL03 CELL(I=1,K=20)
F-LOG d
C-LOG P
F-LOG DZ
C-LOG T
F-LOG MFP
F-LOG TBPM
F-LOG TUM
F
G
LOG(TIME/SEC)

Fig. 8.

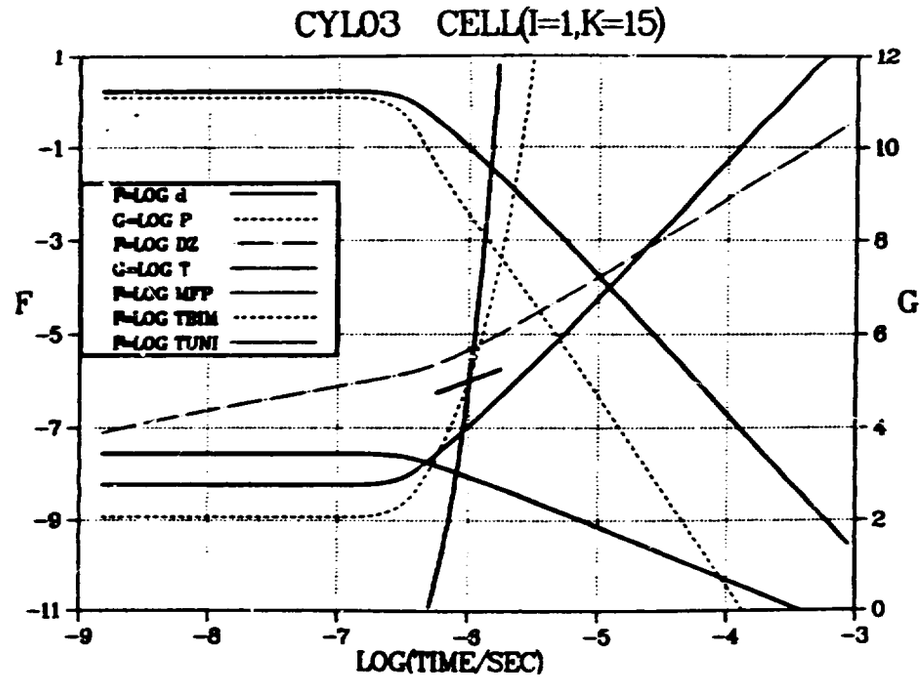
CYL03 CELL(I=1,K=15)
F
G
LOG(TIME/SEC)
F=LOG d
G=LOG P
F=LOG DZ
G=LOG T
F=LOG MFP
F=LOG TBIM
F=LOG TUNI
1
-1
-3
-5
-7
-9
-11
12
10
8
6
4
2
0
-9
-8
-7
-6
-5
-4
-3

Fig. 9.

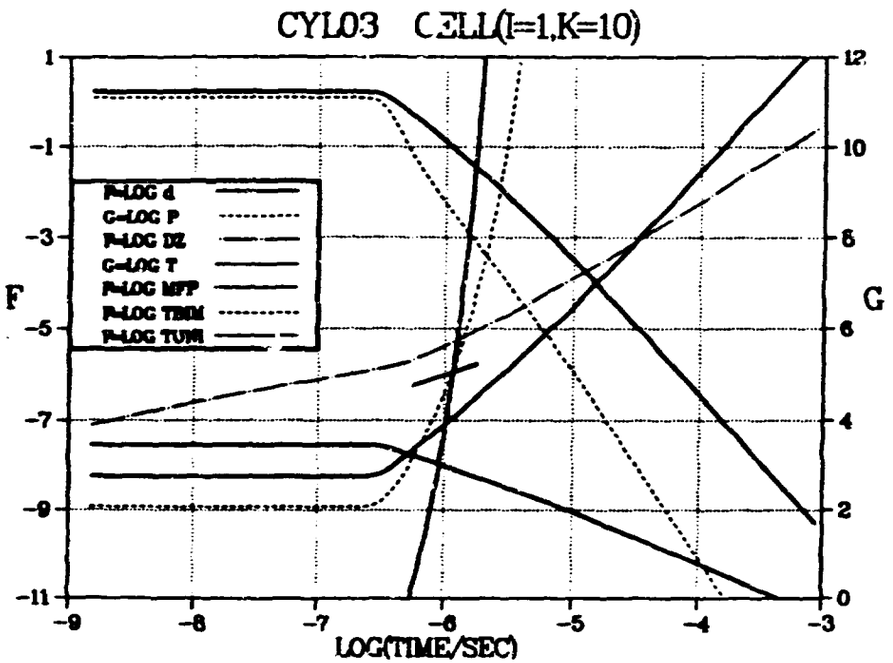
CYL03 CELL(I=1,K=10)
F=LOG d
G=LOG P
F=LOG DZ
G=LOG T
F=LOG MFP
F=LOG TBDM
F=LOG TUM
F
G
LOG(TIME/SEC)
1
-1
-3
-5
-7
-9
-11
12
10
8
6
4
2
0
-9
-8
-7
-6
-5
-4
-3

7:9.10.

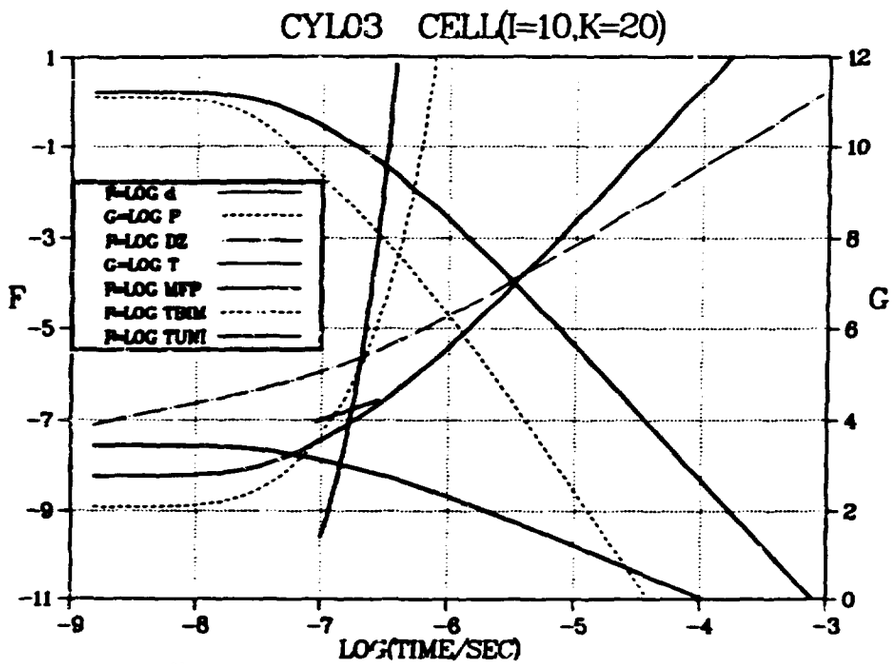
CYL03 CELL(I=10,K=20)
F-LOG d
G-LOG P
F-LOG DZ
G-LOG T
F-LOG MFP
F-LOG TBIM
F-LOG TUM
F
G
LOG(TIME/SEC)
1
-1
-3
-5
-7
-9
-11
12
10
8
6
4
2
0
-9
-8
-7
-6
-5
-4
-3

Fig. 11.

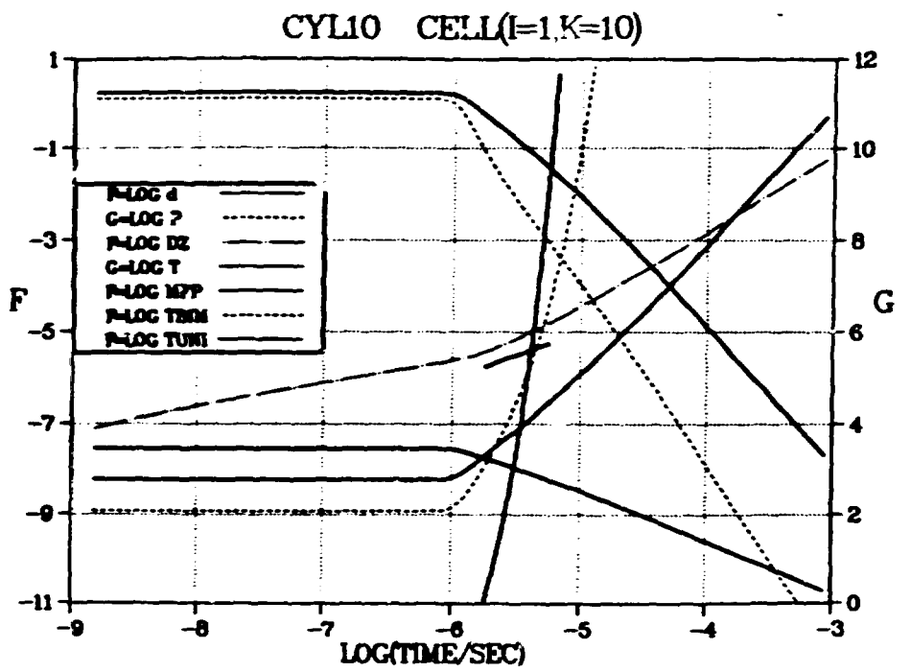
CYL10 CELL(I=1,K=10)
F
G
LOG(TIME/SEC)
F=LOG d
G=LOG ?
F=LOG DZ
G=LOG T
F=LOG M2P
F=LOG TRM
F=LOG TUM
1
-1
-3
-5
-7
-9
-11
12
10
8
6
4
2
0
-9
-8
-7
-6
-5
-4
-3

Fig. 12

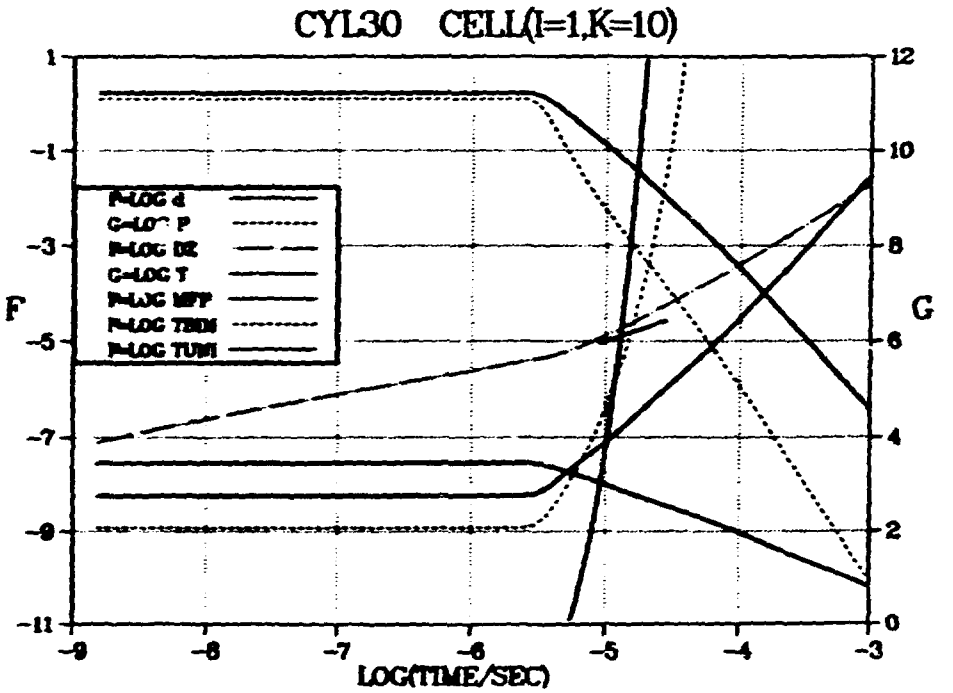
CYL30 CELL(I=1,K=10)
F
G
LOG(TIME/SEC)
1
-1
-3
-5
-7
-9
-11
12
10
8
6
4
2
0
-9
-8
-7
-6
-5
-4
-3

Fig. 13.